

Energy & Environmental Science

Accepted Manuscript

This article can be cited before page numbers have been issued, to do this please use: Z. Fang, J. Zhang, P. Zhu, Z. Yu, A. Elgazzar, J. Wang, W. P. Lam and H. Wang, *Energy Environ. Sci.*, 2026, DOI: 10.1039/D6EE01132B.



This is an Accepted Manuscript, which has been through the Royal Society of Chemistry peer review process and has been accepted for publication.

Accepted Manuscripts are published online shortly after acceptance, before technical editing, formatting and proof reading. Using this free service, authors can make their results available to the community, in citable form, before we publish the edited article. We will replace this Accepted Manuscript with the edited and formatted Advance Article as soon as it is available.

You can find more information about Accepted Manuscripts in the [Information for Authors](#).

Please note that technical editing may introduce minor changes to the text and/or graphics, which may alter content. The journal's standard [Terms & Conditions](#) and the [Ethical guidelines](#) still apply. In no event shall the Royal Society of Chemistry be held responsible for any errors or omissions in this Accepted Manuscript or any consequences arising from the use of any information it contains.

Broader Context Statement

Decarbonizing energy and industrial systems requires carbon capture technologies that combine low energy consumption, operational durability, and scalable process integration. Electrochemical carbon capture has emerged as a promising alternative to thermally driven regeneration because it can directly couple electricity with sorbent regeneration under mild conditions. However, many existing systems rely on large pH gradients between electrodes to release CO₂, which inherently generate significant pH overpotentials, reduce electron efficiency, and increase overall energy demand. Consequently, reactor architecture and interfacial transport management have become critical challenges for translating electrochemical carbon capture into practical deployment. Here, we address this challenge through an integrated reactor design that couples CO₂ absorption with in situ electrochemical CO₂/sorbent regeneration while promoting bicarbonate-mediated capture pathways. This configuration moderates local pH accumulation and maintains effective ionic transport, thereby reducing pH-related energy losses and improving sorbent utilization and electron efficiency during continuous operation. Stable performance at low CO₂ concentrations further supports applicability to flue gas and dilute carbon streams. More broadly, this work demonstrates how reactor-level integration and microenvironment engineering can advance electrically driven carbon capture toward scalable and energy-efficient carbon management technologies.



Efficient and Stable Electrochemical Carbon Capture via Integrated CO₂ Absorption and Regeneration

Zhiwei Fang^{a,*}, Junwei Zhang^a, Peng Zhu^a, Zhou Yu^a, Ahmad Elgazzar^a, Juan Wang^a, Wei Ping Lam^a, and Haotian Wang^{a,b,c,d,e,*}

^a Department of Chemical and Biomolecular Engineering, Rice University, Houston, TX 77005, United States

^b Department of Chemistry, Rice University, Houston, TX 77005, USA

^c Department of Materials Science and NanoEngineering, Rice University, Houston, TX 77005, USA

^d Rice Advanced Materials Institute, Rice University, Houston, Texas 77005, USA

^e Rice WaTER Institute, Rice University, Houston, Texas 77005, USA

*Corresponding authors. E-mail: zf20@rice.edu (Z.F.) and htwang@rice.edu (H.W.)

Supplementary Information available: Figures S1–S27, Tables S1, and supplemental references.

See DOI: 10.1039/x0xx00000x



Abstract

Carbon capture in electrochemical cells generally relies on the local pH differences at the two electrodes, which results in high pH overpotentials and high energy consumption. Here, we integrated CO₂ absorption and *in-situ* CO₂/sorbent regeneration steps in a single electrochemical reactor for reduced energy consumption, simplified process design, and improved reactor stability. By directly feeding carbon source into the cathode chamber while performing CO₂ and sorbent regeneration electrolysis from (bi)carbonate solutions, we successfully demonstrated an in-cell carbon capture and mitigation of local pH elevation, which effectively reduces the pH overpotential and enhances the electron efficiency. Our system enables predominant bicarbonate-based CO₂ capture under point-source conditions, requiring only ~48 kJ mol⁻¹ CO₂ for onset capture and ~180 kJ mol⁻¹ CO₂ at 100 mA cm⁻². This strategy delivers high sorbent utilization efficiency, improved electron utilization, and reduced energy consumption, enabling stable carbon capture operation (3.5% CO₂ concentration input) at 50 mA cm⁻² for over 1,000 hours, with a cation transport efficiency maintained above 80%.



Introduction

As fossil fuels remain a significant part of global energy production and industrial processes, effective mitigation of continuous carbon pollution from different point sources to the atmosphere becomes more urgent than ever. Captured CO₂ can be converted into value-added chemicals, such as carbonates or fuels, or transported to suitable storage sites, where it is securely stored to prevent re-entering the atmosphere.¹⁻³ In recent years, beyond point source capture, direct air capture has started to show its potential in playing an important role in capturing CO₂ directly from the atmosphere, offering the flexibility to locate facilities near renewable energy sources and geological storage sites, and the reliability of carbon feedstock supply chains for certain chemical manufacturing.⁴⁻⁷

Recent advancements in carbon capture, utilization, and storage (CCUS) technologies have led to significant developments in new capture materials and processes, but scaling them up for industrial applications remains challenging.⁷⁻⁹ The widely used chemical absorption method, based on organic amines, is effective but suffers from several major limitations, including solvent degradation and equipment corrosion, highlighting the urgent need for more efficient and stable alternatives. In addition, conventional amine-based CCS systems still require substantial energy input, with parasitic electrical demands of ~30–50 kJ/mol CO₂ and thermal regeneration energies reaching ~2–4 GJ per ton CO₂ (88–176 kJ/mol CO₂).⁹⁻¹² Inorganic alkaline solutions, particularly hydroxide-based systems, present a promising solution for carbon capture, thanks to their high capture efficiency, low material costs due to the abundance of alkali metals, high chemical stability, and good scalability for industrial use.¹³ However, due to the high chemical stability of alkali metal carbonates formed when CO₂ reacts with hydroxides (such as Na₂CO₃ or K₂CO₃), cation exchange with Ca²⁺ is often required to produce CaCO₃, which is then subjected to high-temperature (~ 900 °C) calcination for CO₂ release and sorbent regeneration. While this calcination step is a well-established and widely scaled industrial process, particularly in cement production, its high energy demand and reliance on natural gas as a thermal energy source present significant barriers to large-scale deployment (**Fig. 1a**).³



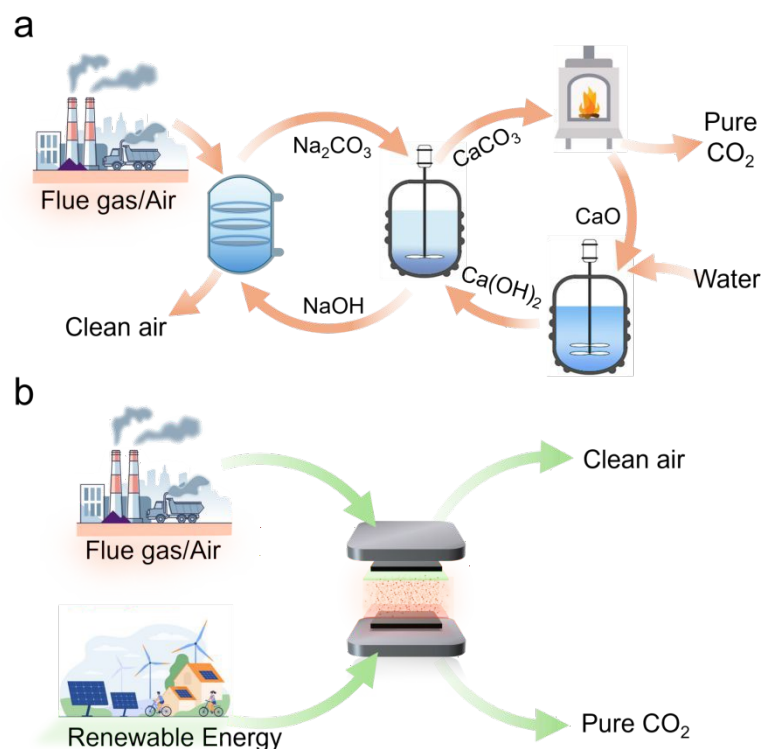


Fig. 1 | Comparison between calcium looping and electrochemical CO₂ capture. (a) Schematic illustration of the pilot-scale CO₂ capture process via calcium carbonate looping. (b) Schematic illustration of the electrochemical CO₂ capture from flue gas or air in our solid electrolyte reactor for complete carbon capture.

Emerging electrochemical methods present a potential breakthrough in addressing the above-mentioned challenges in incumbent carbon capture technologies.¹⁴⁻¹⁹ Instead of relying on high-temperature calcination processes to split metal ions from carbonates for alkaline and CO₂ regeneration, novel electrochemical processes have been demonstrated to effectively split carbonate salts into alkaline sorbent and high-purity CO₂ under room temperature and ambient pressure operations (**Fig. 1b**).^{15, 20} Compared with other electrochemical carbon capture technologies using redox-active organic molecules,⁹⁻¹¹ electrochemical splitting of alkali metal (bi)carbonates (NaHCO₃ or KHCO₃) avoids the use of hazardous, air-sensitive, or poor cycling stability materials. Our recent work on a three-chamber, cation exchange membrane (CEM) based porous solid electrolyte (PSE) reactor demonstrated that electrochemical regeneration can efficiently produce hydroxide and recover CO₂ from absorbents, showing significant advantages compared to the conventional thermal regeneration processes.²¹⁻²³ By flowing (bi)carbonate solutions through the middle PSE layer while carrying out redox reactions at the cathode and



anode, the reactor continuously acidifies the carbonate solution, regenerating high-purity CO₂ from the PSE layer, while simultaneously basifying the cathode chamber as cations are drawn into it.^{24, 25} However, there are still challenges for this approach to be practically implemented.^{19, 26} For instance, in air contactors, the carbon capture process typically halts at the carbonate phase due to the slow reaction kinetics of bicarbonate formation. Regenerating CO₂ from carbonates requires twice the number of electrons compared to bicarbonates, as each carbonate involves the transfer of two protons (H⁺).^{23, 27} This reduces electron efficiency and increases energy consumption.^{23, 27, 28} In another challenge, although the sharp pH gradient between the cathode and anode is needed to generate a chemical potential difference that can be used for CO₂ and sorbent regeneration, this pH difference also contributes to large pH overpotentials that dramatically increase the energy consumption.²³ Therefore, addressing these drawbacks is crucial to further improve the feasibility and energy efficiency of this electrochemical carbon capture method.

In this work, we demonstrated an integrated carbon absorption and regeneration process in a single PSE reactor unit for significantly reduced energy consumption and improved operation stability. By directly feeding CO₂ source gas, typically containing O₂, into the cathode chamber while performing an oxygen reduction reaction (ORR), we leveraged the locally high concentration hydroxides at the cathode/CEM interface for efficient CO₂ absorption as well as hydroxide utilization. Compared with in-cell alkaline generation followed by out-of-cell carbon absorption, this in-cell CO₂ capture design not only simplifies the overall carbon capture process design by eliminating the CO₂ absorption unit, but more importantly, can effectively neutralize the interfacial pH for significantly lowered pH overpotentials and improved Na⁺ transport efficiency (t_{Na^+}). Specifically, at an operation current density of 50 mA cm⁻² and 10% CO₂ concentration for carbon capture, the cell voltage decreased from 1.70 to 1.51 V, while t_{Na^+} increased from 92.6% to 96.0%, representing a 15% improvement in energy consumption. By carefully matching the operational current density with the input CO₂ concentration, we captured carbon from point-source streams (1% to 20%) predominantly in the form of bicarbonate, which delivers ~48 kJ/mol_{CO₂} for onset capture and ~180 kJ/mol_{CO₂} at 100 mA cm⁻² (under 10% CO₂ feed). While performing the same ORR/OER redox electrolysis, this new design represents a ~53% lower



energy input compared to the previously reported anion exchange membrane-proton exchange membrane (AEM-PEM) PSE reactor system,²⁶ which predominantly captures CO₂ via the formation of carbonates, due to significantly enhanced electron efficiency. More importantly, due to the robust chemical stability of CEMs, our CEM-based PSE carbon capture reactor showed excellent long-term reliability, delivering an ultra-stable carbon capture operation at 50 mA cm⁻² for over 1,000 hours while maintaining a transport efficiency of >85% and electron efficiency > 65%. Notably, our approach is also effective for direct air capture with an onset energy consumption of ~52 kJ/mol_{CO₂} and 203 kJ/mol_{CO₂} at 5 mA cm⁻², with an electron efficiency of over 70%. The operational flexibility of the integrated system enables carbon capture to be located near renewable energy sources, providing a pathway to improving overall energy efficiency in CCUS applications.

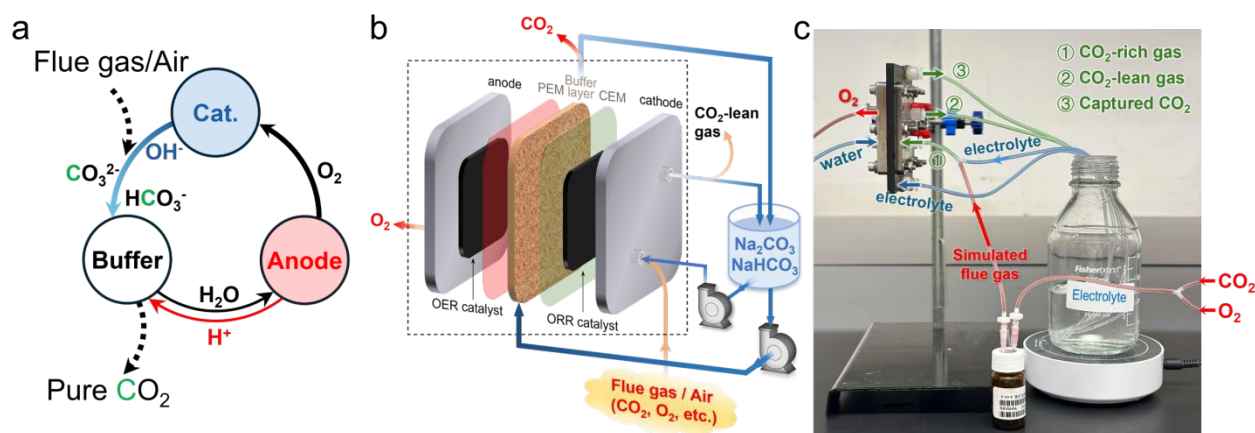


Fig. 2 | Schematic and demonstration of electrochemical CO₂ capture in one solid electrolyte reactor. (a) Process of electrochemical CO₂ absorption and regeneration loop from flue gas or air in our solid electrolyte reactor. (b) Scheme of the electrochemical carbon capture and CO₂ regeneration process. The terms PEM and CEM are used in this work to distinguish their functional roles: PEM is applied when H⁺ transport is desired, whereas CEM is used when Na⁺ is the target cation. (c) Lab-scale electrochemical carbon capture and pure CO₂ regeneration (pump and air flow meters are ignored for simplicity): Green line 1: Pure CO₂ gas / liquid mixture (pH: near neutral or acidic); Green line 2: CO₂-lean gas/ absorbent mixture (pH: near neutral or basic); Green line 3: CO₂-rich gas/ liquid mixture (pH: near neutral or acidic); Blue line: liquid (require the pump to control the liquid flow rate); Red line: gas (require the airflow meter to control the gas flow rate).



Results and discussion

Integrated electrochemical CO₂ absorption and regeneration design

Our system can be implemented for different CO₂ sources, ranging from flue gas capture to DAC. The overall process of the electrochemical CO₂ absorption and regeneration loop is illustrated in **Fig. 2a**. The loop begins with the reduction of oxygen to generate hydroxide ions (OH⁻) at the cathode, which react with CO₂ from the gas feed to form (bi)carbonates. These captured carbon species then flow to a buffer chamber, where they react with protons generated at the anode to release high-purity CO₂ gas. Meanwhile, oxygen is regenerated at the anode and recirculated to the cathode to complete the cycle. Through this loop, CO₂ from flue gas or air is separated into pure CO₂ continuously without any consumption or generation of other chemicals.

The process is facilitated by a three-chamber electrolyzer architecture consisting of a cathode, a PEM-separated buffer chamber packed with a porous solid electrolyte (PSE) layer, and an anode (**Fig. 2b**). At the anode, oxygen evolution reaction (OER, $\text{H}_2\text{O} - 2\text{e}^- \rightarrow 2\text{H}^+ + \frac{1}{2} \text{O}_2$) supplies both protons and oxygen, catalyzed by an OER catalyst. The oxygen produced is recirculated to the cathode, where the oxygen reduction reaction (ORR) occurs on catalysts such as Pt/C or Co single-atom catalysts.²⁹ The ORR generates OH⁻ that reacts with CO₂ to form bicarbonate ($\text{CO}_2 + \frac{1}{4} \text{O}_2 + \frac{1}{2} \text{H}_2\text{O} + \text{e}^- \rightarrow \text{HCO}_3^-$) or carbonate ($\text{CO}_2 + \frac{1}{2} \text{O}_2 + \text{e}^- \rightarrow \text{CO}_3^{2-}$), depending on the capturing conditions. The protons produced at the anode transport across the PEM into the middle buffer chamber, where (bi)carbonates species react with H⁺ to regenerate CO₂ and water ($\text{CO}_3^{2-} + \text{H}^+ \rightarrow \text{HCO}_3^-$, $\text{HCO}_3^- + \text{H}^+ \rightarrow \text{CO}_2 + \text{H}_2\text{O}$). Cations migrate from the buffer chamber to the cathode across the CEM to balance charge. Overall, the electrolyzer converts CO₂ from flue gas or air into high-purity CO₂ (net reaction: CO₂ (flue gas or air) → CO₂ (pure)) without net consumption of chemical sorbents, enabled by coordinated flow, ion transport, and chemical transformations within the cell. The photograph of the electrochemical cell design is depicted in **Fig. 2c**.



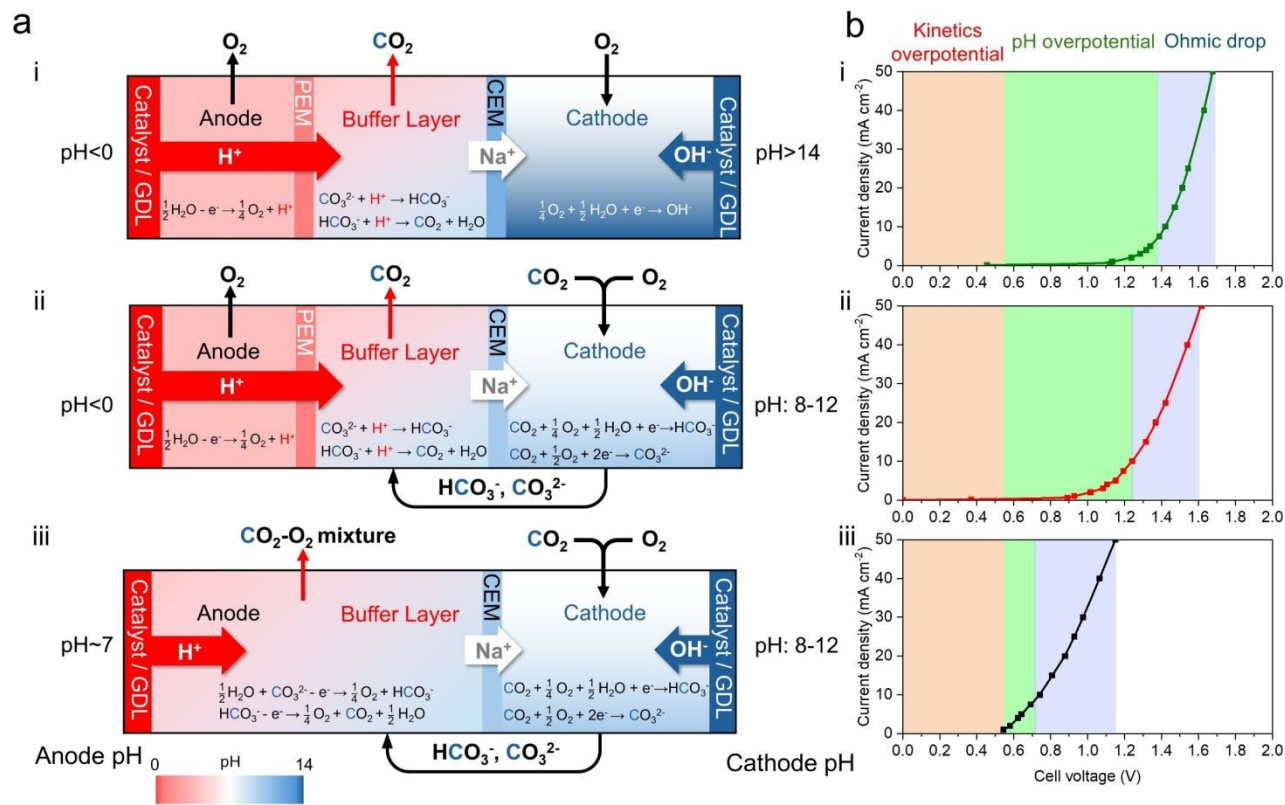


Fig. 3 | Electrolyzer configuration optimization. (a) Schematic of ion movements in three electrolyzers for integrated electrochemical carbon absorption and regeneration process: (i) 3-chamber PSE electrolyzer with pure O₂ feed; (ii) 3-chamber PSE electrolyzer with a CO₂-O₂ mixed feed; (iii) 2-chamber PSE electrolyzer with a CO₂-O₂ mixed feed. (b) Cell voltage breakdowns of three electrolyzers.

For a typical CO₂ regeneration from (bi)carbonates, we compared three different operation cases with different pH overpotentials, as shown in **Fig. 3**. In all three cases, CEM is required to separate the middle chamber and cathode compartment for selective Na⁺ transport (**Supplementary Fig. 4**). The CEM is essential to suppress uncontrolled ion crossover, which would otherwise eliminate the pH gradient and disrupt the decoupled capture-regeneration mechanism, resulting in significant performance degradation. **In the first scenario**, we consider independent CO₂ absorption and regeneration steps. In this case, we do not flow CO₂-containing gas into the cathode chamber, resulting in the generation of alkaline sorbents while a high-purity CO₂ gas stream is regenerated inside the PSE layer from (bi)carbonates. The regenerated alkaline sorbent then flows to the downstream air contactors for the carbon capture process. In this case, we create a sharp pH difference between the anode and cathode interface, and will have the largest pH overpotential during electrolysis operation. **In the second case**, we now include CO₂



in the cathode inlet gas composition (containing both O₂ and CO₂), which reacts with the in-situ generated hydroxide ions right at the cathode/membrane interface to form (bi)carbonates, effectively bringing down the cathode interfacial pH. These carbon-containing ions flow to the middle chamber and react with protons from the anode to release pure CO₂. In this case, the carbon absorption and carbon regeneration steps are integrated and happen simultaneously, and the pH difference between the cathode and anode is reduced due to CO₂-(bi)carbonate buffering effects. **In the third scenario**, since the cathode side interfacial pH now has limited room to be further lowered, we could consider adjusting the anode pH by removing the PEM and forming a two-chamber reactor system. When the PEM in the anode is removed, OER-derived protons are effectively buffered by (bi)carbonates in the PSE layer to form carbonic acid and release CO₂. This will result in an elevated pH at the anode interface, further lowering the pH overpotential of the cell. However, the penalty here is the mixture of the regenerated CO₂ stream with the O₂ stream from OER, which necessitates additional separation processes to isolate pure CO₂ and O₂ for subsequent use or storage. While the CO₂ concentration (80% when considering regenerating bicarbonate, $\text{HCO}_3^- + \frac{1}{2} \text{H}_2\text{O} - e^- \rightarrow \text{CO}_2 + \text{H}_2\text{O} + \frac{1}{4} \text{O}_2$) is significantly improved compared to the cathode feed, this operation mode may find limited application scenarios.

The practical cell voltage ($V_{\text{cell, practical}}$) can be expressed as the following equation:

$$V_{\text{Cell, practical}} = \frac{2.303 \times RT}{F} (\text{pH}_{\text{basified}} - \text{pH}_{\text{acidified}}) + V_{\text{rxn, overpotential}} + iR$$

Where R is the universal gas constant (8.3144 J K⁻¹ mol⁻¹), T is the temperature, F is the Faraday constant (9.6485 × 10⁴ C mol⁻¹). This equation, derived from the Nernst equation, accounts for the pH gradient across the cell. The term $\text{pH}_{\text{basified}}$ refers to the pH at the cathode interface in the basified compartment, while $\text{pH}_{\text{acidified}}$ represents the pH at the anode interface in the acidified compartment.

This equation incorporates three main contributing factors: (1) pH overpotential, (2) catalyst overpotentials for the anodic and cathodic half-reactions (activation energy barriers), and (3) the internal resistance (ohmic drop) of the cell. In this study, $V_{\text{rxn, overpotential}}$ refers to the



overpotentials of anodic OER and cathodic ORR catalysts, while the cell resistance (iR), includes PSE resistance, membrane resistance, and electrode resistance.

In pure CO_2 and sorbent regeneration (case i), PEM and CEM are both utilized with pure O_2 feeding at the cathode, resulting in a highly acidic interface at the anode and a strongly basic flow at the cathode. In case (ii), following the integration of CO_2 absorption into the system, the pH of the cathode flow can decrease due to the direct reaction between the generated OH^- and CO_2 . The pH can be reduced to approximately 8-10 if the captured product is bicarbonate or 11-13 if the product is carbonate. In case (iii), the anode pH can significantly increase after removing PEM at the anode side. Without the PEM as a proton channel, the proton concentration at the anode gradually decreases as protons react with (bi)carbonate ions.

Effects of In-Cell CO_2 Absorption on PSE Electrolyzer Performance

To validate the hypothesis from **Fig. 3** and investigate how CO_2 concentration and current density affect the performance of the PSE electrolyzer, we varied these parameters and evaluated their impact on key metrics such as cell voltage, ion transport efficiency, and pH changes. **Fig. 4a** illustrates the current-voltage (IV) curve and sodium transport efficiency for a three-chamber PSE reactor supplied with a 10% CO_2 feed to the cathode (case ii). At a current density of 50 mA cm^{-2} , the cell voltage is approximately 1.51 V, while at 100 mA cm^{-2} , the cell voltage is increased to 1.75 V. When comparing systems where carbon capture takes place outside the electrolyzer (Pure O_2 feed), the cell voltage is higher than the integrated system. This increase can be attributed to the increased cathodic pH, as shown in Equation (1), due to the existence of hydroxides instead of (bi)carbonates. Additionally, the separated system shows slightly lower cation transport efficiency (**Supplementary Fig. 6 and 7**), which can be attributed to the higher proton crossover from the middle chamber competing with Na^+ (or K^+) transport at high pH without CO_2 . The energy consumption for carbon capture is displayed in **Fig. 4b**, demonstrating that the presence of CO_2 at the cathode lowers the energy inputs due to the synergistic effect of lowered cell voltage and improved Na^+ transport efficiency. The onset energy consumption of 10% CO_2 capture is approximately $50 \text{ kJ/mol}_{\text{CO}_2}$, with average consumption ranging from 140-190 $\text{kJ/mol}_{\text{CO}_2}$ at 50 mA cm^{-2} .



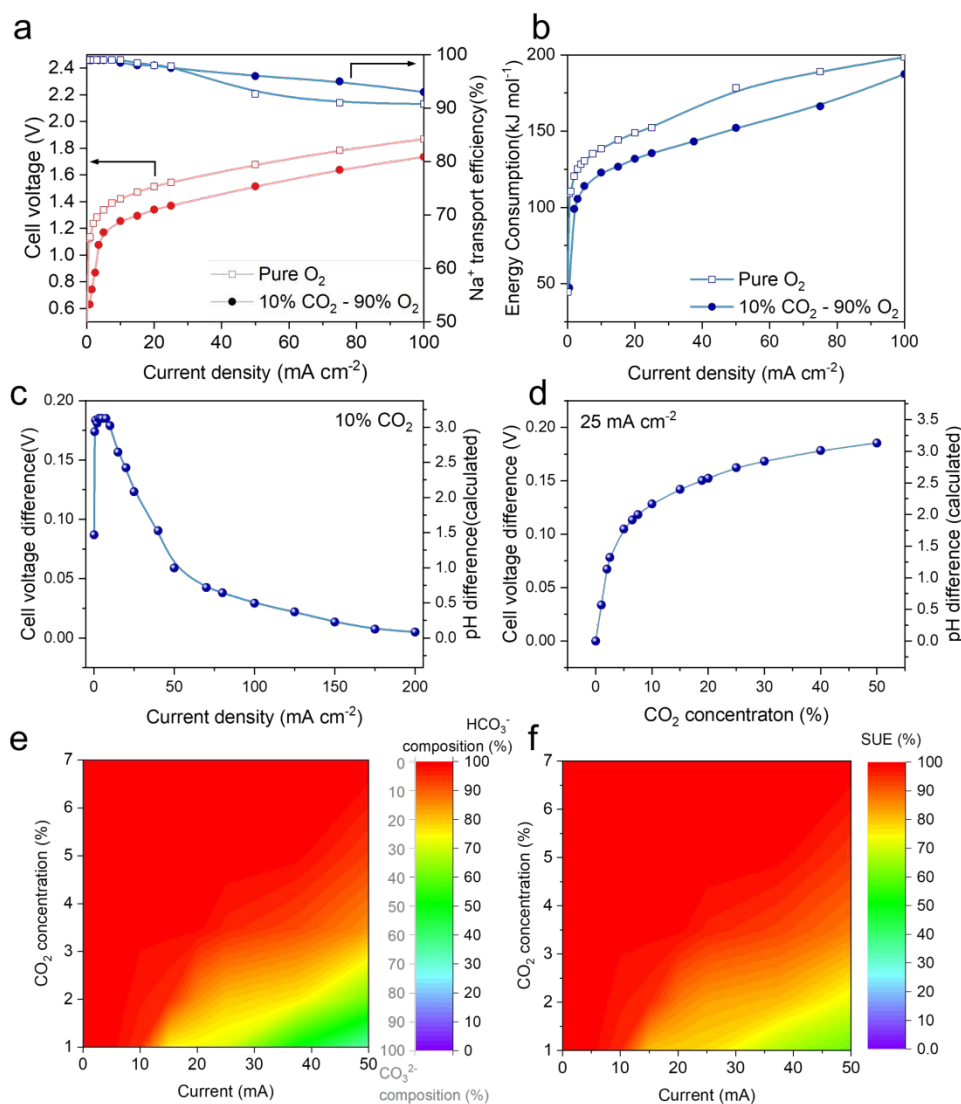


Fig. 4 | CO₂ effect and cathodic pH effect on PSE electrolyzer performance. (a) IV-curve & Na⁺ transport efficiency and (b) energy consumption of PSE electrolyzer feeds with 10% CO₂-90% O₂ and pure O₂. (c) Cell voltage shifts and corresponding cathodic pH differences ($\Delta\text{pH}_{\text{cat}}$) between 10% CO₂ and pure O₂ feeds across varying current densities. (d) Cell voltage shifts and corresponding cathodic pH differences ($\Delta\text{pH}_{\text{cat}}$) at 25 mA cm⁻² across different CO₂ ratios. Here, $\Delta\text{pH}_{\text{cat}}$ represents the difference in cathodic pH between CO₂-fed and CO₂-free (pure O₂) operating conditions. The pH differences were derived from the voltage shifts observed when switching from 0% CO₂ (pure O₂ feed) to different CO₂ concentrations at 25 mA cm⁻². In both (c) and (d), the right-axis pH values were calculated from the left-axis voltage values, and the plotted curve corresponds to both axes. (e) Distribution of captured CO₂ species as a function of CO₂ concentration and currents, and (f) sorbent utilization efficiency (SUE) as a function of CO₂ concentration and currents, originated and processed from experimental data.

According to Equation (2), only the cathodic pH (pH_{cat}) is relevant to the CO₂ concentration. Therefore, the relationship between cell voltage and pH_{cat} is further investigated.



Based on the Nernst equation, the cell voltage difference (ΔV) between CO₂-free (case i in **Fig. 3a**) and CO₂-fed (case ii in **Fig. 3a**) cathodic conditions is given by:

$$\Delta V = \frac{2.303 \times RT}{F} (\text{pH}_{\text{cat, i}} - \text{pH}_{\text{cat, ii}}) \quad (3)$$

Therefore, the cathodic pH difference ($\Delta \text{pH}_{\text{cathode}} = \text{pH}_{\text{cat, i}} - \text{pH}_{\text{cat, ii}}$) between the two conditions can be calculated as $\Delta \text{pH}_{\text{cat.}} = \frac{\Delta V}{0.0591}$. As shown in **Fig. 4c** and **Supplementary Fig. 8**, the pH under 10%-CO₂-fed conditions decreases more significantly at lower current densities, indicating the formation of HCO₃⁻ from OH⁻ and CO₂, and more efficient OH⁻ utilization due to an excess of CO₂ compared to OH⁻. As the current density increases and more OH⁻ is generated, catholyte products gradually change from HCO₃⁻ to CO₃²⁻ due to limited CO₂ mass diffusion. **Fig. 4d** presents the cell voltage and $\Delta \text{pH}_{\text{cat}}$ at various CO₂ concentrations with a fixed current density, demonstrating that increasing CO₂ levels at the cathode helps to push the carbon absorption reaction towards bicarbonate, resulting in lower cell voltages and greater pH drops. The decreasing slope of the upward trend is mainly due to the buffering capacity of (bi)carbonates ions. This demonstrates that current density and CO₂ concentration not only affect capture or sorbent generation rate but also modulate the electrochemical environment within the cell conditions.

To quantify how efficiently the regenerated sorbent is used to capture CO₂ in a single-pass flow through the cathode, we define sorbent utilization efficiency (SUE) as:

$$\text{SUE} = \frac{[\text{NaHCO}_3] + [\text{Na}_2\text{CO}_3]}{[\text{NaOH}]} = \frac{[\text{HCO}_3^-] + [\text{CO}_3^{2-}]}{[\text{Na}^+]} = 1 - \frac{[\text{CO}_3^{2-}]}{[\text{Na}^+]} \quad (3)$$

SUE indicates the chemical form in which CO₂ is captured: A 50% sorbent utilization efficiency corresponds to CO₂ being captured as CO₃²⁻, while a 100% efficiency represents full conversion to HCO₃⁻. Importantly, the SUE obtained in this work from titration (**Supplementary Fig. 9**) reflects only HCO₃⁻ and CO₃²⁻ produced from electrochemically generated OH⁻, excluding contributions from dissolved CO₂ or H₂CO₃. Thus, SUE quantifies only the portion of electrochemical OH⁻ that is converted into bicarbonate or carbonate, not CO₂ that dissolves without consuming OH⁻. When combined with the Na⁺ transport efficiency (t_{Na^+}), which is characterized by the increase in Na⁺ concentration at the cathode, the overall electron efficiency for CO₂ capture (EE_{CO₂}) can be



calculated. EE_{CO_2} , defined as the ratio of captured carbon species to the total electrons used, serves as a key metric for evaluating capture effectiveness.

$$CO_2 \text{ Electron efficiency } EE_{CO_2} = \frac{\text{total captured carbon}}{\text{total } e^-} = \frac{n(HCO_3^-) + n(CO_3^{2-})}{\text{total } e^-} \quad (4)$$

$$EE_{CO_2} = t_{Na^+} \times SUE \quad (5)$$

Assuming $t_{Na^+} = 100\%$, the EE reaches 100% for bicarbonate formation and 50% for carbonate. This difference arises from the reaction stoichiometry: one bicarbonate reacts with one proton (and thus one electron) to form CO_2 , whereas carbonate requires two protons—one to convert to bicarbonate and another to generate CO_2 .

To illustrate how operating conditions influence sorbent utilization efficiency, we quantified bicarbonate composition, defined as the ratio of $n(HCO_3^-)$ to total carbon species (measured by acid titration), across CO_2 concentration and currents, visualizing captured CO_2 species and sorbent utilization efficiency with contour maps generated from experimental data (see more details in **Supplementary Information**). As shown in **Fig. 4e**, higher CO_2 concentrations or lower current densities promote increased HCO_3^- formation. When converted to the sorbent utilization efficiency using Equation (3), **Fig. 4f** shows how sorbent utilization efficiency varies with CO_2 concentration and applied current. Therefore, the cathodic pH difference, which reflects bicarbonate composition and is a key indicator of sorbent utilization efficiency, increases with higher CO_2 concentration but decreases with higher current densities. These results highlight the intrinsic balance between CO_2 concentration, current density, and cell voltage in determining the performance of the PSE electrolyzer. By carefully matching the input CO_2 concentration and the corresponding operation current density, a high sorbent utilization efficiency can be maintained to deliver high electron efficiency in carbon capture.



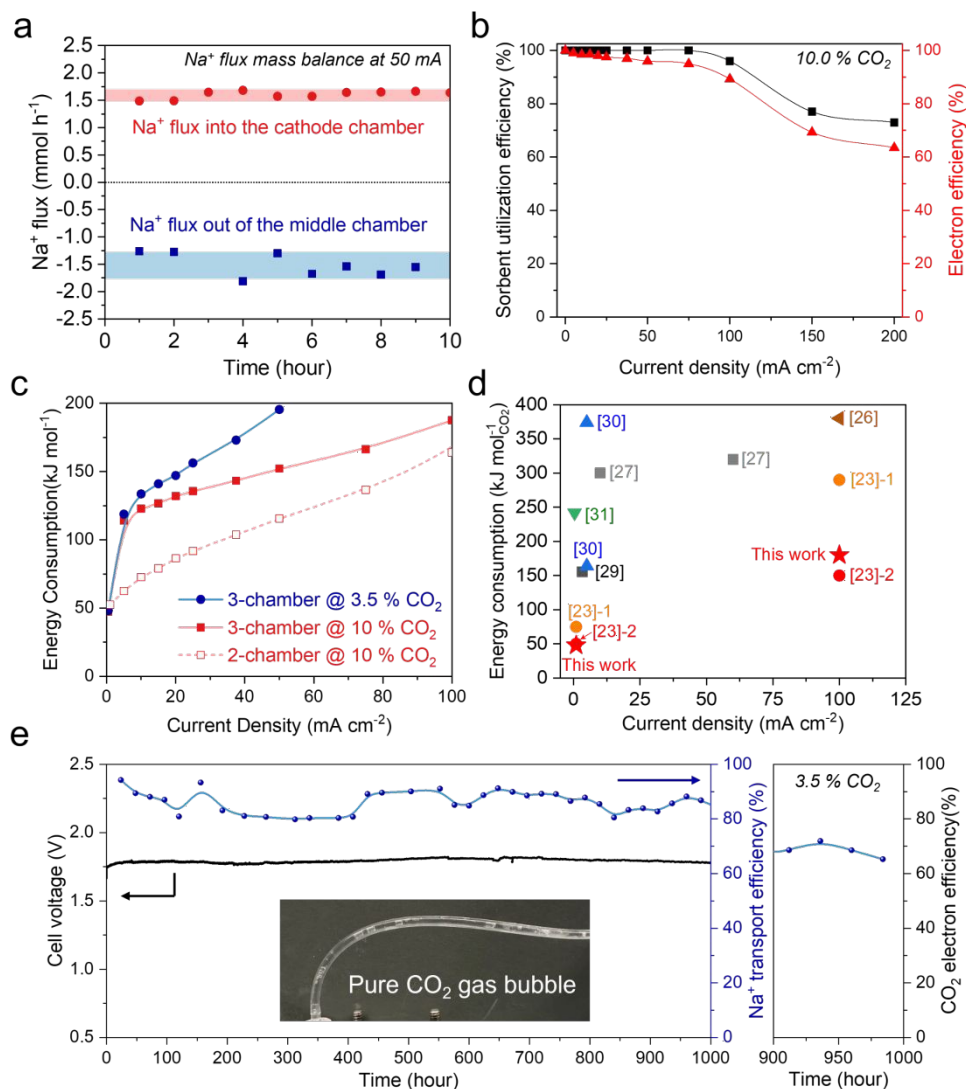


Fig. 5 | Electrochemical characterization and stability of the PSE electrolyzer for point source carbon capture. (a) Na^+ mass balance between the middle PSE layer and the cathode. (b) Sorbent utilization efficiency and electron efficiency for point source capture using 10% CO_2 . (c) Energy consumption for flue gas carbon capture with different concentrations. Onset: $\sim 48 \text{ kJ/mol}_{\text{CO}_2}$; Average: 110-180 $\text{kJ/mol}_{\text{CO}_2}$. 2-chamber PSE configuration shows the lowest pH differences but generates a mixed CO_2/O_2 stream. (d) Comparison of this work and emerging technologies for point source capture: ref [23-1] corresponds to the carbonate feed, and ref [23-2] represents the bicarbonate feed, which leads to lower energy consumption.^{23, 26-28, 30, 31} Detailed parameters are summarized in **Supplementary Tab. 3**. (e) 1000-hour stability with a 3.5% CO_2 feed with a constant current density of 50 mA cm^{-2} . CO_2 electron efficiency is calculated based on the CO_2 regeneration rate from the middle chamber. The 3-chamber PSE cell demonstrated good stability with minimal voltage increase.



PSE Electrolyzer Performance and Stability Study for Carbon Capture

To evaluate the impact of catholyte Na^+ accumulation on reaction efficiency and stability, we first conducted a cation mass balance analysis during the continuous, integrated electrochemical carbon absorption and regeneration process. This involved continuous flow of both the middle buffer chamber stream (1.0 M NaHCO_3 at 60.0 mL h^{-1}) and the cathode stream (1.0 mL h^{-1}), as shown in **Fig. 5a**. At a current of 50 mA , the theoretical increase in Na^+ concentration in the cathode stream is approximately 1.86 mmol h^{-1} , which should be matched by a corresponding Na^+ decrease in the middle PSE layer stream if the cation mass balance is maintained. This value will be around 1.64 mmol h^{-1} when considering a Na^+ transport efficiency of 88% . Based on the ion chromatography result, the Na^+ concentration dropped by $\sim 0.0265 \text{ M}$ in the PSE layer stream, while the concentration in the cathode stream increased by $\sim 1.65 \text{ M}$, corresponding to 1.59 mmol h^{-1} and 1.65 mmol h^{-1} , respectively. The decrease in Na^+ from the PSE layer stream closely matched the amount detected in the catholyte, confirming the Na^+ mass balance between the middle buffer chamber and the cathode. Sorbent utilization efficiency and electron efficiency were evaluated based on the (bi)carbonate species in the catholyte and t_{Na^+} . As shown in **Fig. 5b**, SUE and EE for point source capture using $10\% \text{ CO}_2$ are higher than 60% and 50% at 200 mA cm^{-2} , respectively. To explore the maximum absorbent concentration that our PSE reactor can achieve in the cathode, we performed an additional experiment with a decreased flow rate of catholyte at 200 mA (**Supplementary Fig. 11**). The Na^+ transport efficiency remained stable at $\sim 85\%$ even when producing a Na^+ concentration as high as 5.0 M at a DI water flow rate of 1.3 mL h^{-1} (together with O_2 as the gas input), suggesting that catholyte Na^+ accumulation had no significant impact on cell performance. However, with further reduction in catholyte flow, carbonate salts may crystallize and block the membrane, causing a decrease in the cation transport efficiency, especially considering the theoretical solubility of Na_2CO_3 is only 2.6 M at room temperature.

The advantages of our three-chamber PSE reactor design can be clearly demonstrated by comparing its intrinsic electrochemical performance with other cell configurations. Compared to a conventional 2-chamber membrane electrode assembly (MEA) electrolyzer, where both electrodes directly contact CEM, the middle chamber in the 3-chamber configuration functions



as an important “PSE layer” buffer. The “PSE layer” buffer effectively dilutes proton flux at the anode-membrane interface, reducing the proton competition for Na^+ transport across the CEM by separating the acidic and basic interfaces. Moreover, the PSE layer facilitates good ionic conduction within the middle chamber, promoting Na^+ transport across the CEM. As shown in **Supplementary Fig. 12 and 13**, when replacing the 3-chamber PSE configuration with a 2-chamber MEA configuration, the cell voltages increase drastically, suggesting a repulsion effect at the interface, where protons hinder Na^+ transport.

The anodic pH also significantly influences the cell voltage as discussed above. When the PEM (Nafion membrane) is removed (**Supplementary Fig. 14**), the anode is in a direct contact with the PSE layer, which resulted in a cell voltage decrease of approximately 0.5 to 0.6 V. Elevated temperatures generally accelerate the electrolysis process by increasing ion mobility in the electrolyte and facilitating reactions at the electrode surfaces, leading to increased rates of electrochemical reactions. As shown in **Supplementary Fig. 15**, increased temperature yields lower cell voltage. At 70°C , the cell voltage decreases by approximately 150 mV at 100 mA cm^{-2} , compared with cell voltages at room temperature, indicating enhanced reaction kinetics. The energy consumption for flue gas carbon capture with different concentrations is demonstrated in **Fig. 5c**, with an onset value of $\sim 48 \text{ kJ mol}^{-1} \text{ CO}_2$. 2-chamber PSE configuration shows the lowest pH differences but pays a price in the CO_2 and O_2 mixture. Compared with other emerging technologies for point source capture (**Fig. 5d**), our proposed method shows one of the lowest energy consumptions at higher capture rates.

To evaluate the practical long-term stability of our PSE device for this integrated carbon absorption and regeneration process, we conducted an extended carbon capture experiment (**Fig. 5e**). The stability was evaluated by applying a constant operation current density of 50 mA cm^{-2} , with a 3.5% CO_2 feed at the inlet of the cathode, and 500 mL 1.0 M NaHCO_3 solution as the starting stock solution for the middle chamber during the whole course of stability testing (flow rate: 60 mL h^{-1}). Please note here that this starting carbonate solution can be fully regenerated into CO_2 in 268 hours of operation if no carbon capture is performed to recharge the (bi)carbonate ions. Benefiting from reliable electrocatalysts, membranes, porous solid electrolytes, a less alkaline cathodic condition, and the 3-chamber PSE cell configuration, our



electrolyzer showed excellent stability in capturing CO₂ at the cathode as well as regenerating high-purity CO₂ at the middle chamber. The 3-chamber PSE reactor can be stably operated for more than 1,000 hours, with negligible degradations in both cell voltages (less than 50 mV increase) and t_{Na^+} (maintaining > 80% after 1,000 hours). No additional (bi)carbonates or alkaline solutions were used during the 1,000-hour operation, with pure CO₂ regenerated from the absorbent (Na₂CO₃ and/or NaHCO₃ as captured carbon species), demonstrating the “integrated absorption and regeneration” concept in this study. Under the 50 mA cm⁻² cell electrolysis current, approximately 32.8 mL CO₂ can be stably captured as a pure phase each hour, with an average energy consumption of 235 kJ/mol_{CO₂} (equivalent to 5.3 GJ/ton). The slightly higher energy consumption is mainly attributed to reduced electron efficiency resulting from the lower CO₂ concentration used (3.5% instead of 10%). When scaled up to a 1 m² electrode device, this corresponds to a production rate of approximately 14.2 kg of pure CO₂ per day. Notably, this represents a 33% reduction in energy input when compared to the previously reported AEM-CEM PSE reactor system (~350 kJ/mol_{CO₂} under a similar CO₂ capture rate).²⁴

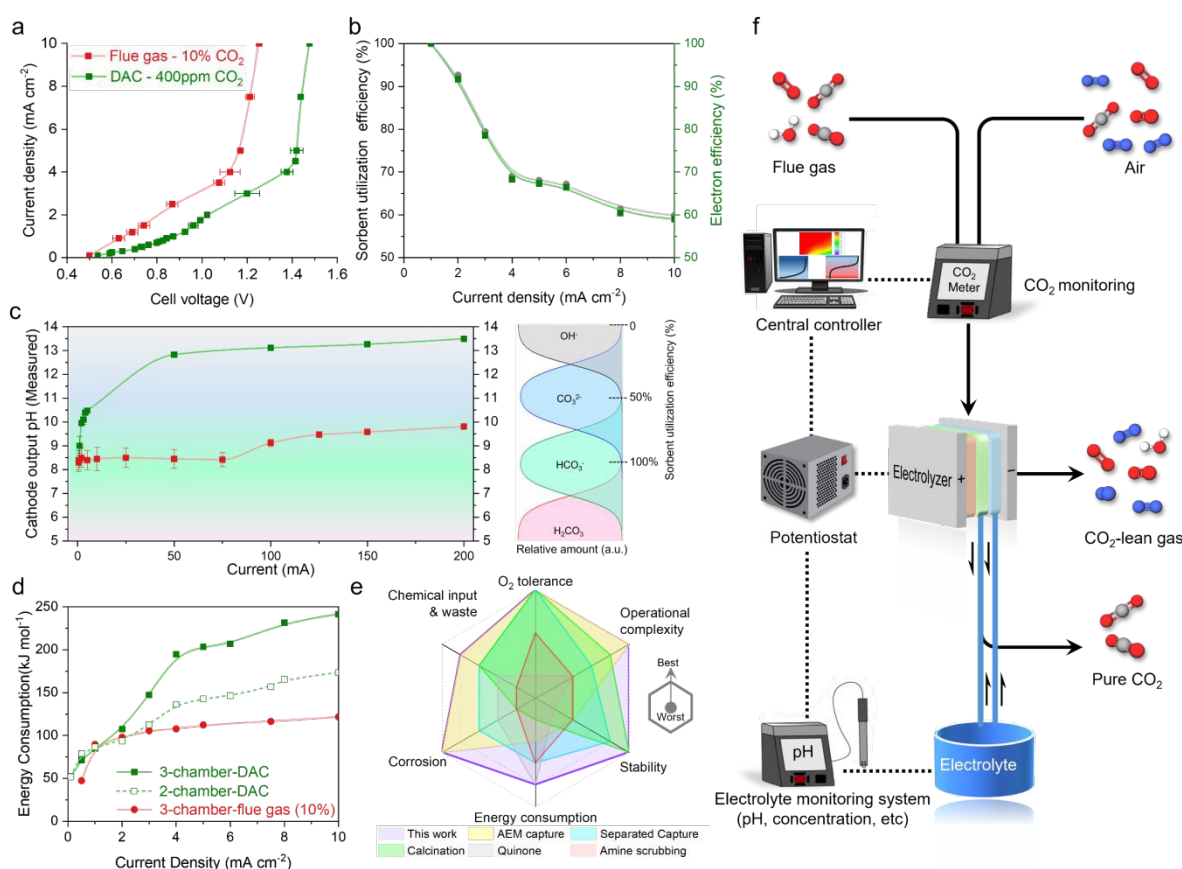


Fig. 6 | PSE electrolyzer for direct air capture. (a) I-V curves of PSE electrolyzers for CO₂ capture from 10% CO₂ feed gas and atmospheric CO₂. The flue gas capture shows lower cell voltage at the same current density, attributed to decreased pH at the cathode after CO₂ capture. (b) Sorbent utilization efficiency and electron efficiency for DAC. (c) pH-current diagram of the catholyte outlet for CO₂ capture from 10% CO₂ feed gas and atmospheric CO₂. Flue gas capture results in much lower pH at the same current, corresponding to the same OH⁻ concentration. Sorbent utilization efficiency is defined for (bi)carbonates. (d) Energy consumption for direct air capture and flue gas carbon capture. Onset: ~52 kJ/molCO₂; Average: ~150kJ/molCO₂ for 2-chamber PSE and ~200 kJ/molCO₂ for 3-chamber PSE electrolyzer. (e) Comparison of our proposed carbon absorption and regeneration strategy with other methods using radar charts. (f) Schematic of proposed dynamic electrochemical CO₂ capture from flue gas or air in our solid electrolyte reactor. The CO₂ and electrolyte monitoring system, which monitors inlet CO₂ concentration and sorbent utilization efficiency, will be integrated with the potentiostat and central controller to enable dynamic current density control, maintaining electron efficiency and automating the carbon capture process.

Electrochemical Preformation in Direct Air Capture (DAC)

DAC enables the removal of CO₂ directly from the atmosphere, offering a versatile approach to carbon capture independent of emission sources. Building on the robust performance of our PSE device in point source capture, we further explored its applicability for DAC, where atmospheric CO₂ concentrations are significantly lower (~400 ppm). Despite the lower concentration, the same principles of electrochemical reactions and robust architecture of the PSE electrolyzer ensure effective CO₂ capture. Notably, the cathode's operation in oxygen-rich air allows the oxygen generated at the anode to be collected, enabling the co-production of pure O₂ and pure CO₂.

The electrolyzer behavior differs notably when capturing atmospheric CO₂ (400ppm) compared to concentrated CO₂ feed streams (**Fig. 6a** and **Supplementary Fig. 21**). For a given current density, flue gas capture operates at a lower cell voltage than atmospheric CO₂ capture. This difference can be attributed to variations in local pH at the cathode following CO₂ absorption (**Fig. 4d**), where a greater pH shift in the flue gas capture contributes to reduced energy consumption. The sorbent utilization and electron efficiencies for DAC are demonstrated in **Fig. 6b**. Notably, the CEM-based PSE reactor maintains over 99.5% electron efficiency at 1 mA cm⁻² and ~70% at 5 mA cm⁻², demonstrating its flexibility and adaptability for integrated carbon



absorption and regeneration across varying operating conditions. While electron efficiency is lower in DAC compared to point-source capture, this difference primarily arises from the much lower CO₂ concentration in ambient air and the inherently slower capture kinetics. Nonetheless, the high electron efficiency at low current densities highlights the reactor's strong potential for efficient DAC performance. **Fig. 6c** demonstrates that the electron efficiency is closely tied to the pH of the absorbent. If no CO₂ is captured, the catholyte will contain only OH⁻, resulting in an EE of 0%. In contrast, the conversion of bicarbonate requires only one electron per CO₂, compared to CO₃²⁻, which enhances electron efficiency and reduces energy demands. Furthermore, for a fixed current and OH⁻ concentration, flue gas capture results in a more substantial pH drop at the catholyte outlet compared to ambient air capture.

Energy consumptions of the PSE electrolyzer under different conditions are shown in **Fig. 6d**. For DAC, the system shows an onset energy of around 50 kJ/mol_{CO₂} and ~80 kJ/mol_{CO₂} at 1 mA cm⁻². At 5 mA cm⁻² current density, it requires ~150 kJ/mol_{CO₂} for the 2-chamber PSE electrolyzer and ~200 kJ/mol_{CO₂} for the 3-chamber PSE configuration. These results show the higher energy demand of DAC compared to flue gas capture, primarily due to the significantly lower concentration of CO₂ in atmospheric air. The system's operational flexibility makes it well-suited for operation near renewable energy sources and geological storage sites, offering a scalable and energy-efficient pathway for CCUS. Further advancement toward practical scalability and economic viability would require progress in several key areas to reduce the overall energy consumption of DAC systems, including: (i) increasing achievable current density under dilute CO₂ conditions to enhance reaction rates and reduce capital costs, (ii) reducing electrolyzer, membrane, and catalyst costs while improving long-term operational durability, and (iii) increasing retention time through electrode architecture modification or flow channel design to improve sorbent utilization efficiency and energy efficiency under low-concentration feed streams. By coupling reactive absorption, local pH gradients, and electrochemical regeneration within an integrated system architecture, this strategy may reduce reliance on energy-intensive intermediate steps such as thermal regeneration and separate process units. In principle, the proposed integration could lower balance-of-plant complexity, reduce system-level energy losses, and improve compatibility with modular scale-up. While significant advances in materials and



operating conditions are still required, this work highlights a potential pathway toward future low-cost and scalable carbon utilization systems.

A comparison between our approach with conventional CO₂ absorption and regeneration technologies, such as calcium looping and amine scrubbing thermal, as well as three strategies reported in recent literature, is summarized in the radar plot in **Fig. 6e** and **Supplementary Tab. S1**. While energy inputs vary across methods, calcium looping is inherently energy-intensive, and many electrochemical strategies suffer from high energy consumption due to lower sorbent utilization or large pH overpotentials. In contrast, our integrated CO₂ absorption and regeneration approach operates solely on renewable electricity without additional chemical input, requires no additional chemical inputs, and generates no waste or pollutants owing to its closed-loop operation and long-term air stability. Notably, unlike the previously reported AEM system relied on a carbonate-limited pathway with restricted electron efficiency, point-source-only operation, and CO₃²⁻ transport, the integrated Na-driven CEM system enables direct bicarbonate regeneration, decoupled absorption/regeneration, and fundamentally different ion-transport. As a result, the current system lowers energy consumption (~150 vs ~350 kJ mol⁻¹ CO₂), enables practical DAC, achieves up to 90% electron efficiency, and demonstrates >1000 h durability. Unlike traditional methods that separate the carbon absorption from CO₂/sorbent regeneration, our integrated method enables continuous, simultaneous absorption and regeneration of pure CO₂ (99.5%, determined by gas chromatography, **Supplementary Fig. 22**), lowering operational complexity and eliminating complicated pre-/post-treatment such as evaporation or salt-dissolution. This simplification may contribute to lower capital costs. Additionally, compared with a separated system, the integrated system maintains a stable operating voltage, ensuring sufficient Na⁺ crossover and avoiding high voltage peaks that increase energy consumption. Importantly, the process does not involve strong acids or bases and avoids corrosion issues commonly associated with the amine scrubbing process. Overall, the comparison demonstrates the versatility and potential of our PSE device as a sustainable and scalable solution for both industrial and atmospheric CO₂ capture. Future deployment of the PSE electrolyzer will require considerations beyond the single-cell configuration demonstrated here. In multi-cell stacks, uniform electrolyte distribution, controlled pressure drop, effective gas-liquid



management, and parasitic energy demands must be addressed. These challenges can be mitigated by utilizing flow-field and manifold designs that are already established in commercial electrolyzers. Shunt currents can be minimized through appropriate electrical isolation strategies, and parasitic pumping and circulation loads are expected to remain modest due to the system's low pressure drop. The high-purity CO₂ output also enables straightforward integration with downstream CO₂ utilization or storage pathways, supporting practical CCUS implementation. Building on these features, we propose an automated CO₂ capture system that integrates CO₂ and electrolyte monitoring with the potentiostat and central controller (**Fig. 6f**). By adjusting current density in response to inlet CO₂ concentration and sorbent utilization efficiency, the system could maintain high electron efficiency and minimize energy consumption, enabling fully automated and energy-optimized carbon capture.

Conclusion

In conclusion, we have developed a closed-loop, electrochemical system for integrated CO₂ capture and sorbent regeneration that combines high operational stability with significantly reduced energy consumption. By leveraging in-situ generated concentrated hydroxide at the cathode for direct CO₂ absorption and simultaneously regenerating high-purity CO₂ and sorbent, our design eliminates the need for separate absorption and regeneration units, streamlining system architecture and enhancing overall efficiency. Co-feeding CO₂ with air or O₂ lowers the cell voltage and improves cation transport across the cation exchange membrane, further reducing energy consumption. Through careful tuning of current density to match the inlet CO₂ concentration, the system predominantly converts CO₂ into bicarbonate under point-source capture conditions, enhancing electron efficiency and reducing energy consumption. This strategy achieves carbon capture at energy inputs as low as ~48 kJ mol⁻¹ for onset capture and ~180 kJ mol⁻¹ at 100 mA cm⁻² under flue gas conditions (10% CO₂ concentration), and remains effective for direct air capture with comparable performance. The operational flexibility and long-term stability highlight the potential of our system as a scalable and practical solution for low-cost, high-efficiency CO₂ capture.



Methods

Three-chamber PSE cell configuration and electrochemical measurement: The salt splitting and acid/base generation were conducted in a PSE cell. The cell configurations and operating procedures are illustrated in **Fig. 2b and c**. The CEM close to the cathode (cathodic ORR catalysts: Pt/C or Co-SAC on hydrophobic carbon cloth electrode) is Nafion N2100TX or ePTFE reinforced Nafion membrane, and the PEM close to the anode side (anodic OER catalysts on carbon paper, IrO_x or RuO_x on gas diffusion layer electrode) is the Nafion-117 membrane. The active electrode area was 4.0 or 1.0 cm² in this study. In the middle chamber, Diaion (Na) ion exchange resin was employed as the PSE.^{2, 32} The flow rate at the outlet was calibrated using a measuring cylinder. The cathode side was provided with a mixture of gas of different concentrations of O₂ and CO₂ or atmosphere for ORR and CO₂ capture reaction. All the cell voltages in our work were reported without any iR compensation. For the flue gas capture, a simulated flue gas (CO₂, O₂ or atmosphere air) was prepared as the gas input to the reactor system. All gas flow rates were precisely controlled by the mass flow controllers and the concentration of the mixture was measured and recorded by a CO₂ meter (sensor from CO2Meter).^{1, 27} The middle solid-electrolyte layer was continuously flowed with 1.0 ml min⁻¹ of (bi)carbonate electrolyte, and the cathode side was circulated with 1.0 ml h⁻¹ of electrolyte.

Synthesis of SACs: The method used for synthesizing Co-SAC is based on our previously reported method, with some modifications.²⁹ First, 1.0 g of *o*-phenylenediamine, 0.44 g of CoCl₂, and 2.0 g of SiO₂ nanoparticles (10–20 nm, Aldrich) templates were mixed together by using 20 ml 1.0 M HCl solution. Then, the mixed solution was sonicated for 0.5 h and stirred for another 0.5 h. Subsequently, 12 ml of 1.0 M HCl solution, which contains 3.0 g of ammonium peroxydisulfate, that is, (NH₄)₂S₂O₈, was added dropwise into the above-mixed solution with vigorous stirring. After polymerization in an ice bath for nearly one day, the mixture was dried using a rotary evaporator. Then, the dried powder was annealed under Ar atmosphere at 800 °C for 2 h. Finally, the product was treated by alkaline (2.0 M NaOH) and acid (2.0 M H₂SO₄) leaching successively to remove SiO₂ nanoparticles templates and unstable Co-based species, respectively, to obtain the Co-SAC. We used the same method to prepare Ni-SAC. The only difference is that 0.405 g



NiCl₂·6H₂O and 1.0 g SiO₂ were used to synthesize Ni-SAC. Fe-SAC was obtained on the basis of our previous paper.

Contour map generation: To visualize the spatial variation of CO₂ concentration and currents for captured CO₂ species distribution (**Fig. 4e**) and sorbent utilization efficiency (**Fig. 4f**), contour maps were generated using experimental data. For non-uniformly spaced points, Shepard interpolation was applied via the XYZ gridding tool to produce a regular Z matrix. The data were then plotted using the *Contour - Color Fill* option, with color scales and levels adjusted to emphasize the distribution of captured CO₂ species and the orbital utilization efficiency.

Author contributions

Z. F. and H.W. conceived the project and designed the experiments. Z.F., J.Z, P. Z., Z. Y., A. E., J. W. and W. P. L. perform the experimental study. Z.F. and H.W. wrote the manuscript with support from all authors.

Declaration of interests

The authors declare no competing interests.

Data availability

The data that support the findings of this study are available from the corresponding authors upon reasonable request.

Acknowledgments

This work was supported by the David and Lucile Packard Foundation (grant no. 2020-71371) and the Alfred P. Sloan Foundation (grant no. FG-2021-15638).

Notes and references

1. P. Zhu and H. Wang, *Nat. Catal.*, 2021, **4**, 943-951.
2. C. Xia, P. Zhu, Q. Jiang, Y. Pan, W. Liang, E. Stavitski, H. N. Alshareef and H. Wang, *Nat. Energy*, 2019, **4**, 776-785.
3. A. Ozden, F. P. García de Arquer, J. E. Huang, J. Wicks, J. Sisler, R. K. Miao, C. P. O'Brien, G. Lee, X. Wang, A. H. Ip, E. H. Sargent and D. Sinton, *Nat. Sustain.*, 2022, **5**, 563-573.



4. A. Sodiq, Y. Abdullatif, B. Aissa, A. Ostovar, N. Nassar, M. El-Naas and A. Amhamed, *Environ. Technol. Innov.*, 2023, **29**, 102991.
5. L. Shi, Y. Zhao, S. Matz, S. Gottesfeld, B. P. Setzler and Y. Yan, *Nat. Energy*, 2022, **7**, 238-247.
6. L. Jiang, W. Liu, R. Q. Wang, A. Gonzalez-Diaz, M. F. Rojas-Michaga, S. Michailos, M. Pourkashanian, X. J. Zhang and C. Font-Palma, *Prog. Energy Combust. Sci.*, 2023, **95**, 101069.
7. F. M. Brethomé, N. J. Williams, C. A. Seipp, M. K. Kidder and R. Custelcean, *Nat. Energy*, 2018, **3**, 553-559.
8. A. I. Osman, M. Hefny, M. I. A. Abdel Maksoud, A. M. Elgarahy and D. W. Rooney, *Environ. Chem. Lett.*, 2021, **19**, 797-849.
9. Y. Liu, H.-Z. Ye, K. M. Diederichsen, T. Van Voorhis and T. A. Hatton, *Nat. Commun.*, 2020, **11**, 2278.
10. K. M. Diederichsen, Y. Liu, N. Ozbek, H. Seo and T. A. Hatton, *Joule*, 2022, **6**, 221-239.
11. J. M. Barlow and J. Y. Yang, *J. Am. Chem. Soc.*, 2022, **144**, 14161-14169.
12. X. Li, X. Zhao, L. Zhang, A. Mathur, Y. Xu, Z. Fang, L. Gu, Y. Liu and Y. Liu, *Nat. Commun.*, 2024, **15**, 1175.
13. X. Ma, L. Azhari and Y. Wang, *Chem*, 2021, **7**, 2843-2847.
14. K. M. Diederichsen, R. Sharifian, J. S. Kang, Y. Liu, S. Kim, B. M. Gallant, D. Vermaas and T. A. Hatton, *Nat. Rev. Methods Primers*, 2022, **2**, 68.
15. G. Wang, J. Chen, Y. Ding, P. Cai, L. Yi, Y. Li, C. Tu, Y. Hou, Z. Wen and L. Dai, *Chem. Soc. Rev.*, 2021, **50**, 4993-5061.
16. Y. C. Xiao, S. S. Sun, Y. Zhao, R. K. Miao, M. Fan, G. Lee, Y. Chen, C. M. Gabardo, Y. Yu, C. Qiu, Z. Guo, X. Wang, P. Papangelakis, J. E. Huang, F. Li, C. P. O'Brien, J. Kim, K. Han, P. J. Corbett, J. Y. Howe, E. H. Sargent and D. Sinton, *Nat. Commun.*, 2024, **15**, 7849.
17. H. Li, M. E. Zick, T. Trisukhon, M. Signorile, X. Liu, H. Eastmond, S. Sharma, T. L. Spreng, J. Taylor, J. W. Gittins, C. Farrow, S. A. Lim, V. Crocellà, P. J. Milner and A. C. Forse, *Nature*, 2024, **630**, 654-659.
18. S. Jin, M. Wu, Y. Jing, R. G. Gordon and M. J. Aziz, *Nat. Commun.*, 2022, **13**, 2140.
19. S. E. Renfrew, D. E. Starr and P. Strasser, *ACS Catalysis*, 2020, **10**, 13058-13074.
20. A. P. Muroyama, A. Pătru and L. Gubler, *J. Electrochem. Soc.*, 2020, **167**, 133504.
21. T. N.-D. Cao, S. W. Snyder, Y.-I. Lin, Y. J. Lin, S. Negi and S.-Y. Pan, *Ind. Eng. Chem. Res.*, 2023, **62**, 20979-20995.
22. Y. Xu, S. Liu, J. P. Edwards, Y. C. Xiao, Y. Zhao, R. K. Miao, M. Fan, Y. Chen, J. E. Huang, E. H. Sargent and D. Sinton, *Joule*, 2023, **7**, 2107-2117.
23. X. Zhang, Z. Fang, P. Zhu, Y. Xia and H. Wang, *Nat. Energy*, 2025, **10**, 55-65.
24. Z. Fang, P. Zhu, X. Zhang, Y. Feng and H. Wang, *Nat. Chem. Eng.*, 2025, **2**, 142-151.
25. Y. Feng, Y. Park, S. Hao, Z. Fang, T. Terlier, X. Zhang, C. Qiu, S. Zhang, F. Chen, P. Zhu, Q. Nguyen, H. Wang and S. L. Biswal, *PNAS*, 2024, **121**, e2410033121.
26. I. A. Digdaya, I. Sullivan, M. Lin, L. Han, W.-H. Cheng, H. A. Atwater and C. Xiang, *Nat. Commun.*, 2020, **11**, 4412.



27. P. Zhu, Z.-Y. Wu, A. Elgazzar, C. Dong, T.-U. Wi, F.-Y. Chen, Y. Xia, Y. Feng, M. Shakouri, J. Y. Kim, Z. Fang, T. A. Hatton and H. Wang, *Nature*, 2023, **618**, 959-966.
28. A. P. Muroyama and L. Gubler, *ACS Sustain. Chem. Eng.*, 2022, **10**, 16113-16117.
29. Z.-Y. Wu, M. Karamad, X. Yong, Q. Huang, D. A. Cullen, P. Zhu, C. Xia, Q. Xiao, M. Shakouri, F.-Y. Chen, J. Y. Kim, Y. Xia, K. Heck, Y. Hu, M. S. Wong, Q. Li, I. Gates, S. Siahrostami and H. Wang, *Nat. Commun.*, 2021, **12**, 2870.
30. Q. Shu, L. Legrand, P. Kuntke, M. Tedesco and H. V. M. Hamelers, *Environ. Sci. Technol.*, 2020, **54**, 8990-8998.
31. M. D. Eisaman, K. Parajuly, A. Tuganov, C. Eldershaw, N. Chang and K. A. Littau, *Energy Environ. Sci.*, 2012, **5**, 7346-7352.
32. C. Xia, Y. Xia, P. Zhu, L. Fan and H. Wang, *Science*, 2019, **366**, 226-231.



The data that support the findings of this study are available from the corresponding authors upon reasonable request.

